TESTING OF THE MILLIAMPERE BOOSTER PROTOTYPE CAVITY*

R. Heine, Institut für Kernphysik, Johannes Gutenberg-Universität Mainz, Mainz, Germany

Abstract

The Milliampere Booster (MAMBO) is the injector linac for the Mainz Energy-recovering Superconducting Accelerator MESA. MESA is a multi-turn energy recovery linac with beam energies in the 100 MeV regime currently designed and built at Institut für Kernphysik (KPH) of Johannes Gutenberg-Universität Mainz [1]. The main accelerator consists of two superconducting Rossendorf type modules [2–4], while the injector MAMBO relies on normal conducting technology. The MAMBO RF cavities are bi-periodic $\pi/2$ structures [5, 6] with 33 cells and 37 cells, respectively. In this paper we present the results of the commissioning and testing of a 13 cell prototype structure.

INTRODUCTION

In an energy recovery linac (ERL) only the energy provided by the main linac modules can be recovered. So the beam is dumped at injection energy after the recuperation of energy. At MESA the beam dump will be located inside the accelerator hall. Thus the injection energy to the ERL shall be below neutron production threshold of the beam dump material. The injector linac has to be able to provide beam current from some µA up to 1 mA for the experiments P2 [7] and MAGIX [8] at a high quality. In MESA stage-2 the maximum beam current will be extended to 10 mA.

In [9] a normal conducting linac with a graded-β RF-section and three β = const. sections based on the MAMI ILAC concept [10] as well as a hybrid linac where the β = const. sections were replaced by one or two TESLA-type SRF-cavities [11] have been researched. The final design study has been recently published [12]. The Milliampere Booster MAMBO was decided to be a 1.3 GHz normal conducting linac with a final energy of 5 MeV. Then the design was refined w.r.t. longitudinal beam dynamics and RF-design in [13] and [14]. The linac structure (see Fig. 1) is of the bi-periodic $\pi/2$ type [5, 6]. This means that there are two types of cells: long accelerating cells (AC) with electric field inside and short coupling cells (CC) with no field. This geometry increases the shunt impedance (R_s) of the $\pi/2$-mode compared to a simple periodic structure. Since there are two kinds of cells, the $\pi/2$-mode is degenerated. So the passband has a gap g, that needs to be closed by tuning both cell types to the same frequency for stable operation (see [15] for further information).

In [14] some hints for multipacting (MP) were found and investigated which led to the dimensions of the cells listed in Table 1. The cell coupling was increased to $k = 8\%$ which improves field flatness and tuning stability. Further to allow for beam currents of up to 10 mA the beam pipe radius was enlarged compared to the scaled ILAC geometry. Also the
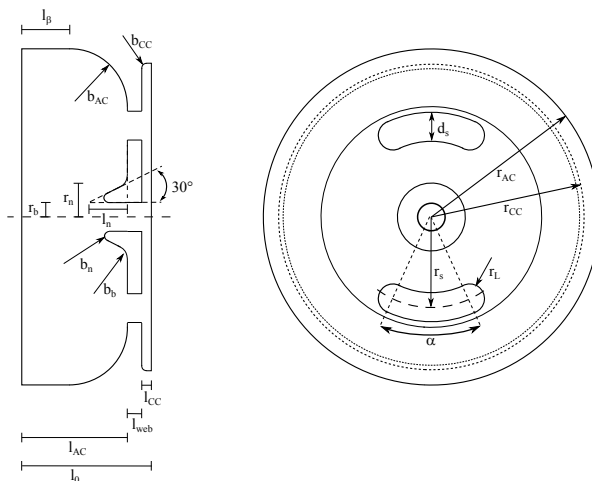
MC2: Photon Sources and Electron Accelerators

A08 Linear Accelerators

Figure 1: Drawing of a segment of the bi-peridic RF-structure. The dimensions are listed in Table 1.

Table 1: Dimensions of the bi-periodic structure (see Fig. 1). The ILAC structure [10] is scaled to 1.3 GHz and then optimised for MAMBO.

	ILAC	Scaled	MAMBO
l_0 (mm)	30.6	57.65	57.65
l_{AC} (mm)	25.748	48.509	46.55
l_{CC} (mm)	1.941	3.657	5.6
l_β (mm)	7.514	14.156	12.16
l_{web} (mm)	2.911	5.484	5.5
l_n (mm)	10.267	19.343	19.3
r_{AC} (mm)	46.749	88.075	86.7
r_{CC} (mm)	43.9625	82.825	77.9
r_b (mm)	6.216	11.712	15
r_n (mm)	12.144	22.879	26.143
r_s (mm)	25.238	47.548	55.15
r_L (mm)	4.996	9.412	12
b_{AC} (mm)	18.234	34.353	34.39
b_{CC} (mm)	0.9	1.696	1.7
b_n (mm)	1.178	2.219	2.22
b_b (mm)	3.386	6.379	6.39
d_s (mm)	11.17	21.044	24
α (°)	35	35	37

accelerating field was lowered to $E_{acc} = 0.66\,\text{MV}\,\text{m}^{-1}$ to improve MP behaviour and thus the number of cells of the sections was increased compared to [13]. The final design of the four MAMBO cavities is denoted in Table 2.

PROTOTYPE RF-SECTION

In order to test the RF-design, cooling concept, frequency control and MP behaviour under real conditions, it was decided to build a prototype RF-section. The design criteria

Table 2: Design data of the four MAMBO RF-sections. The cavities have been simulated with CST Studio. To match the cell lengths to the particle velocity l_{AC} is scaled with β. The cavity losses have been calculated for $E_{\mathrm{acc}} = 0.66\,\mathrm{MV\,m^{-1}}$.

	β	R_s (MΩ)	R/Q (kΩ)	Q_0	P_c (kW)	κ	AC	CC	L_{eff} (mm)
MAMBO 1	0.579 … 0.958	46.7	2.2	20500	41	1.3	19	18	1 860.2
MAMBO 2	0.977	99.3	4.3	22900	18.8	1.6	17	16	1 914.88
MAMBO 3	1.0	103.4	4.4	23400	19.3	1.6	17	16	1 960.1
MAMBO 4	1.0	103.4	4.4	23400	19.3	1.6	17	16	1 960.1

was to reach $E_{\mathrm{acc}} \approx 1\,\mathrm{MV\,m^{-1}}$ with the MESA 15 kW solid state power amplifier (SSPA) [16] available. So a $\beta = 1$ cavity with 13 cells and critical coupling ($\kappa = 1$) was designed. The figures of the prototype are listed in Table 3.

Table 3: This table lists the data of the MAMBO prototype RF-section. The R_s of the actual resonator was calculated from Q_0.

AC : CC	7 : 6		CST	Exp.
f_0 (MHz)	1300	Q_0	23500	20938 $\pm$ 503
L_{eff} (mm)	807.1	R_s (MΩ)	42.8	37.7 $\pm$ 0.5
R/Q (kΩ)	1.8	κ	1	0.94

Since solenoid focussing of $B_{\mathrm{sol}} = 100\,\mathrm{G}$ is needed over MAMBO 1 to enable beam currents exceeding $I_b = 1\,\mathrm{mA}$, a prototype solenoid was installed on the RF-section to check for MP that, according to simulation, might be induced by the magnetic field.

The MAMBO prototype was manufactured by "RI research instruments GmbH", Bergisch Gladbach and delivered in January 2018. As RF-window a Thales TH20698A was used. The Solenoid ($n = 1061$) is air cooled and produces B_{sol} at $I_{\mathrm{sol}} = 2.1\,\mathrm{A}$. The coil was wound at "Jelonnek Transformatoren und Wickelgut GmbH", Oberkochen. The tuners have been made in house and are compatible to the MAMI frequency control system that was used with a 1.3 GHz RF-front end for controlling the resonance frequency. The prototype was installed and tested at the SRF test bunker [17] at the "Helmholtz Institut Mainz" (HIM). A picture of the setup can be seen in Fig. 2.

LOW POWER TESTING

At low power several measurements were performed. The tuning range of the plungers was measured and found to be in good agreement with simulation. The Q_L of the $\pi/2$-mode was measured to be $Q_L = 10793 \pm 260$ and is as expected ca. 10 % lower than simulation.

There is a change of the passband gap Δg under thermal load. It has two portions: a temporal Δg_t and a permanent one Δg_p. The later persists after the first high power operation and has to be taken into account during pre-braze tuning. It was found that the passband gap is not independent of the tuner position. This is because the passband modes have different amplitudes in the tuner cells and therefore react differently to the change of volume introduced by the plunger. So Δf of each mode is different and thus changes
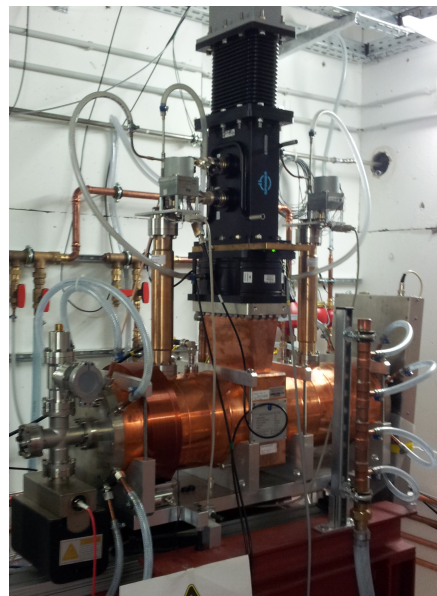

Figure 2: Prototype at HIM test bunker.

the shape of the passband and also g. To determine Δg_p for series production, the passband was recorded at several tuner positions p before high power processing and afterwards (see Fig. 3). For $p < 0$ where the plunger is moving out of the cavity into a pipe, $g(p)$ is not linear any more due to the pipe being a cut-off. To find Δg_p straights were fitted to $g(p)$ for $p > 0$. The difference of the y-intercepts yields $\Delta g_p = 750\,\mathrm{kHz}$.
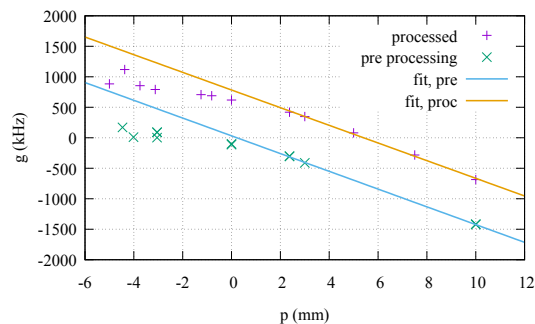

Figure 3: Passband gap g before and after high power processing as function of the plunger position p. The permanent change of the gap was calculated by subtracting the y-intercept of both linear fits.

MC2: Photon Sources and Electron Accelerators

A08 Linear Accelerators

HIGH POWER TESTING

With a generator power of P_g = 15 kW and the given R_s a field E_{acc} > 0.9 MV m^{-1} can be built up in the cavity. This is well above the accelerating gradient needed for MAMBO and therefore sufficient to test for any limitation of the design.

Prior to processing the cavity was heated to ϑ = 65 °C for two weeks to support desorption of water during evacuation. The temperature was chosen to be below the maximum storage temperature of the RF window to not risk breakage.

The cavity was processed in CW operation. Maximum E_{acc} was reached after a net processing time of only 9.3 h without any problems or signs of multipacting. The diagram in Fig. 4 shows the vacuum as a function of the accelerating field $p(E)$ during high power processing. The pressure break outs are correlated to an increase of field. One can see how over time the vacuum improves at a certain E_{acc}.
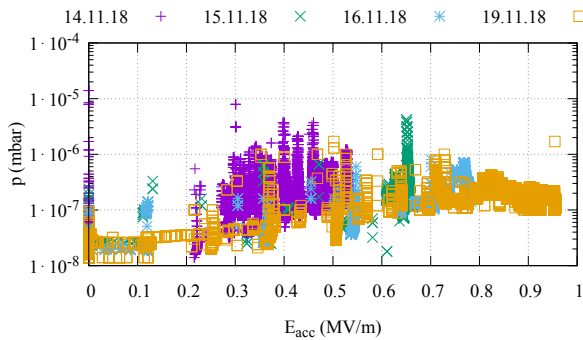
Figure 4: Vacuum pressure p as a function of accelerating field E. The solenoid field is switched off.

Next, processing was repeated with B_{sol} = 100 G. A basic automatic processing routine was implemented and used for this. The routine periodically checked for vacuum pressure and increased the input power of the SSPA by 0.1 dBm if the vacuum was better than 2×10^{-7} mbar. With this routine maximum field was reached after 45 min. In Fig. 5 $p(E)$ with B_{sol} > 0 is shown. One finds that there is some vacuum activity around E = 0.2 MV m^{-1} to 0.4 MV m^{-1}. During research of the effect by varying E_{acc} and B_{sol} the vacuum activities decreased and could not be detected any more. The orange curve in Fig. 5 shows a typical behaviour of the prototype where pressure starts to increase from 1.4×10^{-8} mbar to $\approx 4 \times 10^{-8}$ mbar when E_{acc} exceeds 0.5 MV m^{-1}. With B_{sol} switched off $p(E)$ behaves the same. Comparing Figs. 4 and 5 one can see that the vacuum pressure at maximum E_{acc} is still improving.

After venting the prototype to change a vacuum valve in summer 2019, there was some fluctuation in cavity power and reflected power found during reprocessing. The process was frequency dependent (see Fig. 6) and was gone for $E \gtrsim$ 0.3 MV m^{-1} (P_c > 2 kW). It was independent of B_{sol}. Hence being frequency dependent and a low power effect, it might be MP. Possibly some contamination was introduced
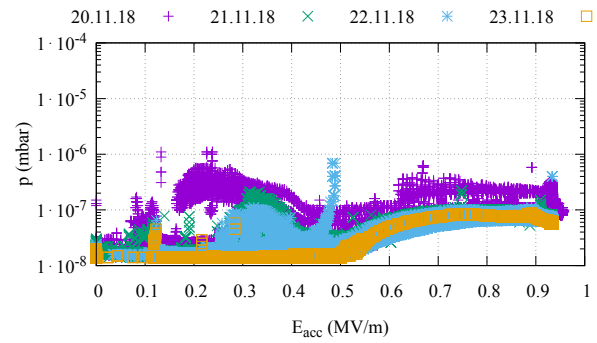
Figure 5: Vacuum pressure p as a function of accelerating field E. The solenoid field is switched on.
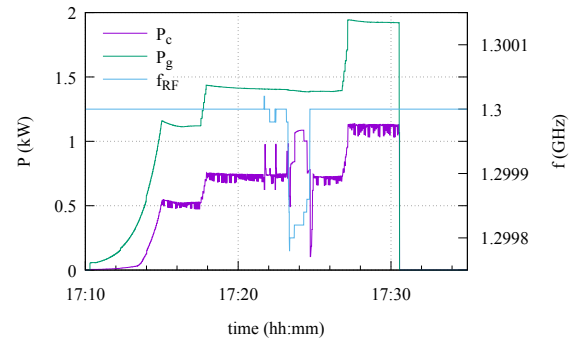
Figure 6: Frequency dependent fluctuation of cavity power P_c while generator power P_g is stable.

during venting. So baking before reprocessing after vacuum breaking seems mandatory for future operation.

So MP simulations were revisited to model those effects. Three possible areas of MP could be identified: at the base of the nose cones, in the slit of the power coupler and in the coaxial structure formed by the plunger and its pipe. At the nose cones simulation found MP with a longitudinal B-field and $E \gtrsim$ 0.2 MV m^{-1}. Maybe this is the cause of the vacuum activities found with B_{sol}, which could be processed. The tuner had MP onset at 0.3 MV m^{-1} with B-field and 0.4 MV m^{-1} without. This might explain the pressure increase found at E_{acc} > 0.5 MV m^{-1}. The coupler showed MP at $E \gtrsim$ 0.7 MV m^{-1} independent of B. The threshold behaviour found during processing could not be verified and therefore the origin of the observed effect remains unclear.

SUMMARY & OUTLOOK

A normal conducting prototype RF-section for the MESA injector linac MAMBO was successfully tested at low power as well as at high power. Important operational experience with the RF-design was gained. The four RF-sections for MAMBO based on the design tested were tendered in spring 2019 and are currently in production at RI. Commissioning of the MAMBO RF-sections is expected for 2022.

REFERENCES

[1] F. Hug *et al.*, "Status of the MESA ERL Project", in *Proc. 63rd Advanced ICFA Beam Dynamics Workshop on Energy Recovery Linacs (ERL'19)*, Berlin, Germany, Sep. 2019, pp. 14-17. doi:10.18429/JACoW-ERL2019-MOCOXBS05

[2] J. Teichert *et al.*, "RF Status of Superconducting Module Development Suitable for CW Operation: ELBE Cryostats", *Nucl. Instr. Meth. A*, vol. 557, pp. 239-242, Feb. 2006. doi:10.1016/j.nima.2005.10.077

[3] T. Stengler *et al.*, "Modified ELBE Type Cryomodules for the Mainz Energy-Recovering Superconducting Accelerator MESA", in *Proc. 17th Int. Conf. RF Superconductivity (SRF'15)*, Whistler, Canada, Sep. 2015, paper THPB116, pp. 1413-1416.

[4] T. Stengler *et al.*, "Status of the Superconducting Cryomodules and Cryogenic System for the Mainz Energy-recovering Superconducting Accelerator MESA", in *Proc. 7th Int. Particle Accelerator Conf. (IPAC'16)*, Busan, Korea, May 2016, pp. 2134-2137. doi:10.18429/JACoW-IPAC2016-WEPMB009

[5] D. E. Nagle, E. A. Knapp, and B. C. Knapp, "Coupled Resonator Model for Standing Wave Accelerator Tanks", *Rev. Sci. Instrum.*, vol. 38, p. 1583, 1967. doi:10.1063/1.1720608

[6] E. A. Knapp, B. C. Knapp, and J. M. Potter, "Standing Wave High Energy Linear Accelerator Structures", *Rev. Sci. Instrum.*, vol. 39, p. 979, 1968. doi:10.1063/1.1683583

[7] D. Becker *et al.*, "The P2 Experiment", *Eur. Phys. J. A*, vol. 54, p. 208, 2018. doi:10.1140/epja/i2018-12611-6

[8] S. Baunack, "Low Energy Accelerators for High Precision Measurements", presented at Electromagnetic Interactions with Nucleons and Nuclei Conference (EINN), Paphos, Cyprus, Oct.-Nov. 2017, unpublished.

[9] R. G. Heine and K. Aulenbacher, "Injector Linac for the MESA Facility", in *Proc. 4th Int. Particle Accelerator Conf. (IPAC'13)*, Shanghai, China, May 2013, paper WEPWA011, pp. 2150-2152.

[10] H. Euteneuer, H. Braun, H. Herminghaus, R. Klein, H. Schoeler, and T. Weis, "The Injector Linac for the Mainz Microtron", in *Proc. 1st European Particle Accelerator Conf. (EPAC'88)*, Rome, Italy, Jun. 1988, pp. 550-553.

[11] B. Aune *et al.*, "Superconducting TESLA Cavities", *Phys. Rev. ST Accel. Beams*, vol. 3, p. 092001, Sep. 2000. doi:10.1103/PhysRevSTAB.3.092001

[12] R. Heine, "Preaccelerator concepts for an energy-recovering superconducting accelerator", *Phys. Rev. Accel. Beams*, vol. 24, p. 011602, Jan. 2021. doi:10.1103/PhysRevAccelBeams.24.011602

[13] R. G. Heine, K. Aulenbacher, S. Friederich, C. Matejcek, and F. Schlander, "Further Investigations on the MESA injector", in *Proc. 6th Int. Particle Accelerator Conf. (IPAC'15)*, Richmond, VA, USA, May 2015, pp. 1515-1517. doi:10.18429/JACoW-IPAC2015-TUPWA045

[14] R. G. Heine, K. Aulenbacher, L. M. Hein, and C. Matejcek, "Current Status of the Milliampere Booster for the Mainz Energy-recovering Superconducting Accelerator", in *Proc. 7th Int. Particle Accelerator Conf. (IPAC'16)*, Busan, Korea, May 2016, pp. 1741-1743. doi:10.18429/JACoW-IPAC2016-TUPOW002

[15] T. P. Wangler, *RF Linear Accelerators*, Second ed., Darmstadt, Germany: Wiley-VCH, 2007.

[16] R. G. Heine and F. Fichtner, "The MESA 15 kW cw 1.3 GHz Solid State Power Amplifier Prototype", in *Proc. 9th Int. Particle Accelerator Conf. (IPAC'18)*, Vancouver, Canada, Apr.-May 2018, pp. 4216-4218. doi:10.18429/JACoW-IPAC2018-THPMF063

[17] F. Hug *et al.*, "Cryogenic Installations for Module Tests at Mainz", in *Proc. 19th Int. Conf. RF Superconductivity (SRF'19)*, Dresden, Germany, Jun.-Jul. 2019, pp. 997-1002. doi:10.18429/JACoW-SRF2019-THP054